Dynamical tuning of the thermal conductivity via magnetophononic effects

Claudio Cazorla [1,*] and Riccardo Rurali [2,†]

[1] *Departament de Física, Universitat Politècnica de Catalunya, Campus Nord B4-B5, Barcelona 08034, Spain*

[2] *Institut de Ciència de Materials de Barcelona, ICMAB–CSIC, Campus UAB, 08193 Bellaterra, Spain*

(Received 5 May 2021; revised 13 December 2021; accepted 16 February 2022; published 1 March 2022)

Strategies for tuning the thermal conductivity of crystals by means of external fields are rare. Here, we predict the existence of large magnetophononic effects in materials that undergo antiferromagnetic (AFM) ↔ ferromagnetic (FM) phase transitions, which allow for the modulation of the lattice heat conductivity, κ_L, via the application of magnetic fields. Specifically, by using first-principles methods we predict a large and anomalous κ_L increase of ≈40% for the metamagnetic phase transition occurring in bulk FeRh near room temperature. The disclosed magnetophononic effects are caused by large anharmonic spin-phonon couplings, namely, significant differences in the phase space of allowed phonon-phonon collision processes taking place in the respective AFM and FM phases.

DOI: 10.1103/PhysRevB.105.104401

I. INTRODUCTION

Phonons, or quanta of lattice vibrations, are quasiparticles that carry heat in crystals. Efficient manipulation of phonons by external fields, therefore, should allow for dynamical control of the lattice thermal conductivity of solids, κ_L. Yet, to a large extent, dynamical tuning of κ_L remains to this day a fundamental and technical challenge. It is sometimes argued that the main hurdle in this endeavor is the absence of a net phonon mass or charge [1]. However, this type of reasoning can be easily challenged by phase-change arguments: whenever the application of an external field produces crystal structure variations, the accompanying lattice vibrations should also change, thus inducing potential κ_L modifications. In fact, recently it has been shown that it is possible to act upon the κ_L of ferroelectric perovskites via the application of electric fields that either write/erase domain walls [2–6] or produce symmetry-breaking cationic displacements [7–11]. Likewise, the charge density of a silicene single-layer can be redistributed via electric fields in such a way that the phonon-phonon interactions are significantly affected [12].

In this context, a stimulating question naturally arises: is it possible to achieve similar dynamical control of κ_L in other predominant families of functional materials like magnetic crystals? For the *magnetophononic* response of a magnetic crystal to be sizable, we envisage that the following general conditions need to be met: (i) the switching between two (or more) magnetic states driven by a magnetic field should be possible (i.e., experimentally demonstrated and/or predicted by advanced theories); (ii) the competing magnetic phases should exhibit distinct crystal structures (e.g., symmetry and/or volume) and spin-phonon couplings in order to maximize their lattice vibrational differences [13–15]; and (iii) although not compulsory from a fundamental point of view, it is desirable that the involved magnetic transformation occurs near room temperature (i.e., to envisage possible technological applications).

In this paper, we predict the existence of novel and sizable magnetophononic effects in bulk FeRh (i.e., a κ_L variation of ∼40% upon switching of magnetic states), a well-known magnetocaloric and mechanocaloric [16–19] material that fulfills conditions (i)–(iii) above. Bulk FeRh exhibits a cubic CsCl crystal structure (space group $Pm3m$, Fig. 1) and at a temperature of $T_M \sim 350$ K it undergoes a magnetoisostructural transition from a low-T antiferromagnetic (AFM) phase to a high-T ferromagnetic (FM) phase [20]. In the AFM (FM) phase, the Rh magnetic moments are null ($1.0\mu_B$) and the Fe magnetic moments remain large (i.e., $\sim 3.0\mu_B$ [21,22]; see Table I). The magnetoisostructural phase transition is accompanied by a large volume increase ($\Delta V/V \sim 1\%$ [20]; Table I). Despite the fact that the crystal symmetry of FeRh is preserved during the AFM ↔ FM transformation, the phonon spectra of the two magnetic competing states are quite different [23,24], thus indicating that the two phases are considerably different already at the harmonic vibrational level. Furthermore, (i) FeRh is an archetypal multicaloric compound with a large vibrational entropy change associated with its metamagnetic phase transition (i.e., $|\Delta S_L| \approx 30$ J K^{-1} kg^{-1} [25]), and (ii) the AFM → FM transformation can be triggered near room temperature via the application of small magnetic fields (∼1 T [16,20]), thus validating our materials choice. It is worth mentioning that similar AFM ↔ FM phase transitions exist also in a wide variety of other materials such as multiferroic $SrMnO_3$ [26] and (Zn,Sn,Mn)As_2 thin films [27], bulk $LaCrGe_3$ [28] and USb_2 [29], and the solid solutions $Ce(Fe_{1-x}Al_x)_2$ [30] and $Mn_2Sb_{1-x}Bi_x$ [31]. Thus, the magnetophononic effects disclosed here are of broad physical interest.

II. COMPUTATIONAL METHODS

We performed density-functional theory (DFT) calculations using the VASP code [32] and projector augmented waves

*claudio.cazorla@upc.edu

†rrurali@icmab.es

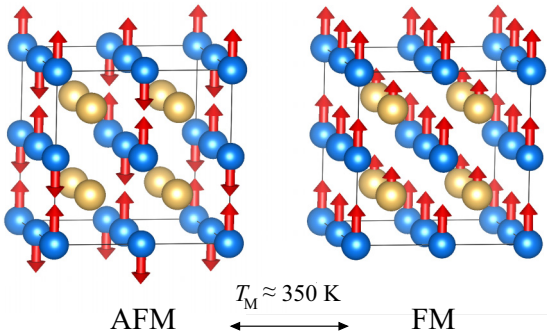

FIG. 1. Sketch of the AFM (left) and FM (right) phases of bulk FeRh. Fe and Rh ions are represented with blue and orange spheres, respectively. The arrows represent the Fe and Rh magnetic moments. The unit cell of the AFM phase is $2 \times 2 \times 2$ times larger than that of the FM phase due to accommodation of the corresponding antiferromagnetic type-G ordering.

[33,34] with an energy cutoff of 450 eV. The generalized-gradient approximation to the exchange-correlation functional along with the revised Perdew, Burke, and Ernzerhof parametrization (revPBE) [35] were used. The first Brillouin zone (IBZ) of the FM two-atom unit cell was sampled with a Monkhorst-Pack [36] grid of $26 \times 26 \times 26$ **k**-points centered at Γ. AFM type-G ordering requires a 16-atom unit cell to be reproduced (Fig. 1), thus in this case a **k**-point grid of $13 \times 13 \times 13$ was consistently employed. Table I encloses some computed physical parameters like the lattice parameter and ionic magnetic moments, which in general are in very good agreement with the available experimental data. The adopted computational approach is also able to provide a reasonable estimate of T_M and the T-H phase diagram of bulk FeRh within the quasiharmonic approximation [37] (see the discussion in Sec. III). It is worth mentioning that a monoclinic $P2/m$ structure has been recently predicted by Wolloch *et al.* to be competitive at low temperatures [23]; however, this FeRh phase has eluded experimental confirmation thus far and hence we have not considered it in our analysis. It has also been theoretically suggested that a small tetragonal distortion could play a role in determining the ground state of FeRh, which might be AFM type-A′ [38]. These conclusions are valuable because under certain experimental conditions the tetragonal symmetry could be favored. However, there is wide consensus (including Ref. [38]) in that only the magnetic states AFM type-G and FM magnetic are stable (or metastable) in cubic FeRh, which is the crystal symmetry observed under normal conditions. Notice also that FeRh has been reported to become paramagnetic at 670 K [39], that is, roughly 300 K above the temperature of the metamagnetic transition discussed here. Therefore, T-induced spin-disorder effects have been safely neglected in our first-principles calculations.

TABLE I. Unit-cell lattice parameter, volume, and ionic magnetic moments estimated for FeRh in the FM and AFM phases at zero temperature. The volume change $\Delta V/V$ computed for the FM phase is relative to that of the AFM ground state. "DFT" stands for the present computational work, and "expt" for experimental data reported in the literature.

	FM_{DFT}	FM_{expt}	AFM_{DFT}	AFM_{expt}
a (Å)	3.025		6.018	6.000 [22]
V (Å^3/f.u.)	27.68		27.24	27.00 [22]
$\Delta V/V$ (%)	1.6	∼1 [20]		
m_{Fe} (μ_B)	3.1	∼3.0 [21]	3.1	3.3 [21]
m_{Rh} (μ_B)	1.0	∼0.6 [21]	0.0	0.0 [21]

The second- and third-order interatomic force constants (IFCs) were calculated by finite differences [40,41] in a $4 \times 4 \times 4$ supercell for the FM phase and in a $2 \times 2 \times 2$ supercell for the AFM phase. We considered interactions up to sixth nearest neighbors in three-phonon scattering processes (see Sec. V for details on how the symmetry breaking introduced by AFM spin ordering was treated in our calculations and its consequences). The IFCs were then used as inputs to solve the phonon Boltzmann transport equation (BTE) beyond the relaxation time approximation (RTA), using the iterative algorithm implemented in the ShengBTE code [41]. The BTE was solved on a **q**-point grid of $16 \times 16 \times 16$ for FM FeRh and of $8 \times 8 \times 8$ for AFM FeRh, after conducting careful convergence studies. The lattice thermal conductivity was calculated as

$$\kappa_{L,ij} = \frac{1}{k_B T^2 \Omega N} \sum_{\lambda} f_{\lambda}^0 \left(f_{\lambda}^0 + 1\right) (\hbar\omega_{\lambda})^2 v_{i,\lambda} F_{j,\lambda}$$
$$= \frac{1}{N} \sum_{\lambda} C_{\lambda} v_{i,\lambda} F_{j,\lambda}, \quad (1)$$

where indexes i and j run over the three Cartesian directions, k_B, T, Ω, and N are the Boltzmann constant, temperature, volume of the unit cell, and number of **q**-points, respectively, and C_{λ} is the volumetric heat capacity of the phonon mode λ [42] (i.e., the volumetric heat capacity of the crystal is $C_P = 1/N \sum_{\lambda} C_{\lambda}$). The sum runs over all the phonon modes, and λ comprises both the wave vector **q** and the branch index p. f_{λ}^0 is the equilibrium Bose-Einstein distribution function, $\hbar$ is the reduced Planck constant, and ω_{λ} and $v_{i,\lambda}$ are the phonon frequency and phonon group velocity, respectively. $F_{j,\lambda}$ takes the general form $\tau_{\lambda}(v_{j,\lambda} + \Delta_{j,\lambda})$, where τ_{λ} is the relaxation time and Δ_{λ} is the correction over the RTA. It is worth stressing that since our main goal here is to compare the lattice thermal conductivity of FM and AFM FeRh, both magnetic phases were computationally treated on exactly the same footing (i.e., the same supercell size, nearest-neighbor cutoff for anharmonic phonon-phonon processes, and **k**-point grid for IBZ sampling).

III. QUASIHARMONIC FREE-ENERGY CALCULATIONS: ESTIMATION OF THE AFM ↔ FM PHASE TRANSITION TEMPERATURE AND T-H PHASE DIAGRAM OF BULK FeRh

First-principles Gibbs free-energy calculations were conducted within the quasiharmonic approximation (QHA) for bulk FeRh in the described cubic AFM and FM phases to theoretically determine the value of some fundamental T-dependent quantities, thus assessing the reliability of the employed density functional theory (DFT) approach via

comparison with the available experimental data. The fundamentals of the DFT-QHA method can be found in many previous works (e.g., Refs. [19,37]) and are briefly summarized next.

The Gibbs free energy of a given solid phase, $G_{\rm harm}$, can be expressed as

$$G_{\rm harm}(P,T) = E(P) + PV(P,T) + F_{\rm harm}(P,T), \quad (2)$$

where E is the static energy of the system (i.e., as directly obtained from zero-temperature DFT calculations), P is the pressure, V is the volume, and $F_{\rm harm}$ is the lattice Helmholtz free energy. (The dependence of the different energy terms on P and T has been explicitly noted.) Within the QHA, for a given V and T the value of $F_{\rm harm}$ is determined by using the formula

$$F_{\rm harm}(V,T) = \frac{1}{N_q} k_B T \sum_{\mathbf{q}s} \ln\left[2\sinh\left(\frac{\hbar\omega_{\mathbf{q}s}(V)}{2k_{\rm B}T}\right)\right], \quad (3)$$

where $\omega_{\mathbf{q}s}$ are the phonon frequencies obtained at the reciprocal lattice vector $\mathbf{q}$ and phonon branch s, and N_q is the total number of wave vectors used for integration in the Brillouin zone. At the same time, the hydrostatic pressure P is calculated via the expression

$$P(V,T) = -\frac{\partial[E(V) + F_{\rm harm}(V,T)]}{\partial V}, \quad (4)$$

which numerically allows for determining $V(P,T)$. Thus, by performing E and $\omega_{\mathbf{q}s}$ DFT calculations for a set of V points (over which interpolation is applied to continuously describe the selected interval) and using Eqs. (2)–(4), it is possible to estimate $G_{\rm harm}(P,T)$. Finally, to determine the temperature at which the AFM $\leftrightarrow$ FM phase transition occurs at a given P, T_M, we use the condition $\Delta G_{\rm harm}(P,T_M) \equiv G^{\rm AFM}_{\rm harm}(P,T_M) - G^{\rm FM}_{\rm harm}(P,T_M) = 0$. [Note that the QHA formalism described in Sec. III neglects magnetic entropy contributions stemming from spin fluctuations and also possible spin-phonon coupling effects [37]. Nonetheless, such approximations are expected to have a very minor impact on our T_M predictions since FeRh is observed to become paramagnetic at very high temperatures (i.e., 670 K [39] whereas $T_M \sim 350$ K [20]).] It is worth noting that the present DFT-QHA formalism allows for consideration of volumetric thermal expansion effects in the calculation of Gibbs free energies, which represents a physical improvement with respect to purely harmonic models. In what follows, we restrict our analysis to the zero-pressure case.

On the technical side, we computed the value of the energies E and $F_{\rm harm}$ for the FeRh AFM and FM phases under 0%, 1%, 2%, and 3% homogeneous expansive strains. The static DFT energies were interpolated for an arbitrary volume by using a Birch-Murnaghan equation of state [37], while the vibrational free energies were interpolated by using second-order polynomials of the volume at each temperature (at the same time, the temperature was scanned at a frequency of 1 K within the interval $200 \leqslant T \leqslant 500$ K). Importantly, customary DFT energy functionals are known to provide excessively large static energy differences among the AFM and FM phases of FeRh (i.e., $\Delta E^{\rm DFT} = 43.2$ meV/f.u. in the present case) as compared to the experimental evaluation of the same quantity (i.e., $\Delta E^{\rm expt} = 5.38$ meV/f.u. [23]). Such a ΔE overestimation leads to unrealistically high T_M values predicted within the described DFT-QHA scheme (i.e., $T_M > 1000$ K). To overcome such a computational limitation in practice, Wolloch *et al.* proposed to use the experimental $\Delta E^{\rm expt}$ value in combination with the computed $\Delta F_{\rm harm}$ energies [i.e., to employ the condition $\Delta G^*(T_M) \equiv \Delta E^{\rm expt} + \Delta F_{\rm harm}(T_M) = 0$ at null pressure] [23], and in the present work we have followed that same recipe.

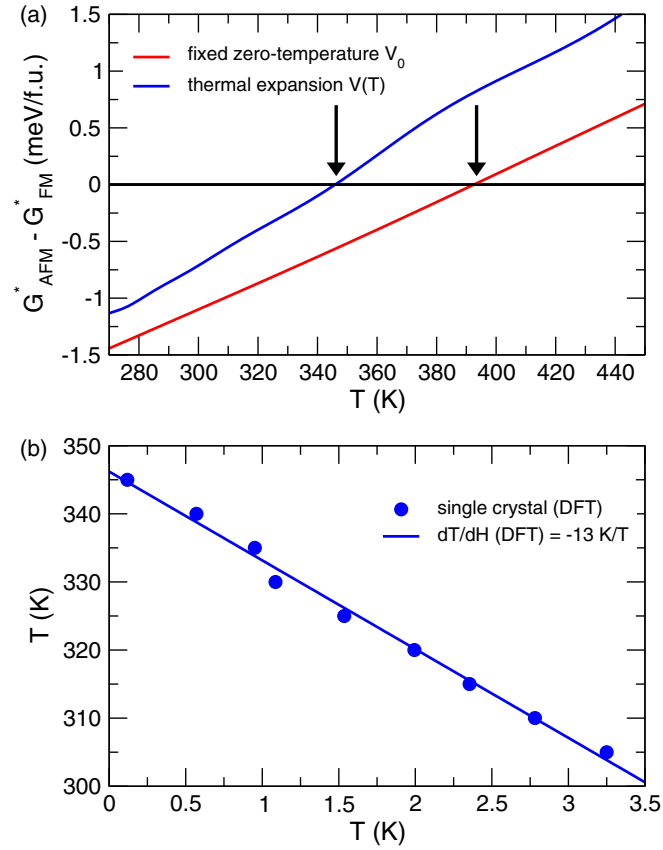

FIG. 2. First-principles quasiharmonic free-energy calculations of FeRh in the AFM and FM bulk cubic phases at zero pressure. (a) DFT estimation of Gibbs free energies obtained by neglecting/considering thermal expansion effects and adopting the experimental zero-temperature energy difference among the two phases. The resulting AFM $\leftrightarrow$ FM transition temperatures are highlighted with black arrows. (b) DFT estimation of the T-H phase diagram of bulk FeRh (in a single-crystal and single-domain configuration) obtained by considering thermal expansion effects and adopting the experimental zero-temperature energy difference among the two phases. Solid dots represent the actual DFT results, whereas the solid line is a linear fit to them.

Figure 2(a) shows the results of our zero-pressure DFT-QHA ΔG^* calculations for bulk FeRh by considering and neglecting volumetric thermal expansion effects. When the volume of the AFM and FM phases estimated at zero temperature is constrained in the calculations, rather than the pressure, we obtain a T_M value of 390 (10) K, which is in good agreement with previous analogous DFT calculations by Wolloch *et al.* [23]. Meanwhile, when volumetric thermal expansion effects are adequately taken into consideration, our estimation of T_M amounts to 345 (10) K, which is in very close agreement with the experimental value $T_M^{\rm expt} \sim 350$ K [20,23].

These results, therefore, lead to the expected conclusion that considering T-induced V variations may improve the prediction of phase-transition temperatures.

The DFT-QHA free-energy approach described here also allows for an approximate estimation of the T-H phase diagram of bulk FeRh, where H represents the external magnetic field that is necessary to trigger the AFM → FM phase transition at temperatures $T \leqslant T_M$. In particular, since the net magnetization of the AFM phase is zero, to a first approximation one can assume that the minimum H that is required to stabilize the FM phase over the AFM amounts to

$$H(T) = -\frac{\Delta G^*(T)}{M(T)} = \frac{G^*_{\mathrm{FM}}(T) - G^*_{\mathrm{AFM}}(T)}{M(T)}, \qquad (5)$$

where $M(T)$ represents the net magnetization of the FM phase. In the particular case of bulk FeRh, since T_M is much lower than the temperature at which the crystal becomes paramagnetic [39], one can reasonably simplify the involved calculations by assuming that $M(T) \approx M(0)$, which according to our DFT estimations is equal to $M = 4.1\mu_B$ (see Table I).

Figure 2(b) shows the first-principles T-H phase diagram deduced for bulk FeRh considering a single-crystal and single-domain configuration (e.g., effects derived from the presence and coexistence of interacting magnetic domains are totally disregarded) by using the formulas and method described above. It is found that the rate of T_M variation as induced by the presence of modest magnetic fields is quite constant and approximately equal to $dT/dH = -13$ K/T. The closest physical system for which an analogous experimental T-H phase diagram has been reported is, to the best of our knowledge, epitaxial FeRh films (see, for instance, Ref. [43]). Despite the obvious physical differences among the simulated bulk single-crystal single-domain system and epitaxial FeRh films (e.g., in the latter system the lattice parameters are slightly strained in comparison to those of bulk, and many interacting magnetic domains and boundaries exist), the agreement between the corresponding T-H phase diagrams can be regarded as reasonably good. In particular, the experimental H-induced T_M variation reported in Ref. [43] exhibits also a clear linear behavior and the boundary slope amounts to $dT/dH^{\mathrm{expt}} = -8$ K/T.

In view of the bulk T_M and T-H phase diagram results presented in this section, it can be concluded that the first-principles computational method adopted in the present study, although not without some limitations, can provide a reasonably accurate description of the metamagnetic AFM ↔ FM phase transition occurring in FeRh near room temperature.

IV. THERMAL CONDUCTIVITY OF FeRh IN THE AFM AND FM MAGNETIC PHASES

The phonon dispersion and vibrational density of states of cubic AFM and FM FeRh are shown in Fig. 3. It is clear that already at the harmonic level, the AFM and FM phases are very different. In the AFM phase, the symmetry reduction originated by antiparallel magnetic moments results in the lifting of several phonon degeneracies and widening of the corresponding phase space (potentially leading to enhanced phonon scattering). The volumetric expansion occurring from

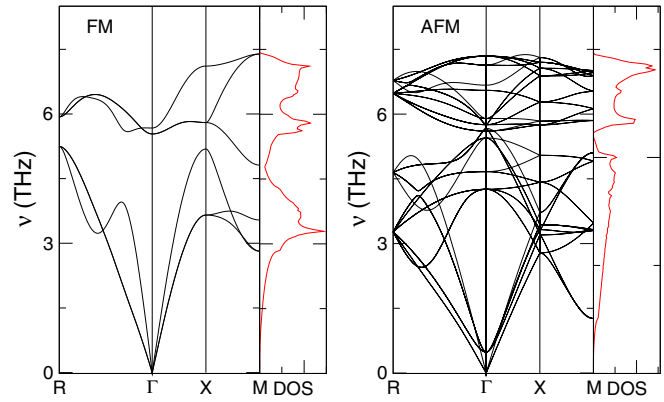

FIG. 3. Phonon dispersion and vibrational density of states (VDOS) calculated for FM and AFM FeRh. The doubling of the AFM unit cell results in a larger number of phonon modes and the lifting of several phonon degeneracies as compared to those of the FM phase. The high-symmetry reciprocal-space points are R ($\frac{1}{2}$, $\frac{1}{2}$, $\frac{1}{2}$), Γ (0,0,0), M ($\frac{1}{2}$,0,0), and X ($\frac{1}{2}$, $\frac{1}{2}$,0) in units of π/a, where $a_{\mathrm{FM}} = 3.025$ Å and $a_{\mathrm{AFM}} = 6.018$ Å and thus $q^{\Gamma\to R,X}_{\mathrm{FM}} \approx 2q^{\Gamma\to R,X}_{\mathrm{AFM}}$.

the AFM → FM phase transition, on the other hand, leads to an overall softening of the FM phonon modes throughout the Brillouin zone. We will come back to this point later, but for now it is instructive to compare the group velocities, $\delta\omega_k/\delta\mathbf{q}$, calculated for the acoustic modes of the two magnetic phases near Γ: along the $R \to \Gamma$ direction $v^a_{\mathrm{AFM}} = 2670$ and 5898 m/s and $v^a_{\mathrm{FM}} = 2320$ and 5549 m/s, and along the $\Gamma \to X$ direction $v^a_{\mathrm{AFM}} = 3600$ and 4950 m/s and $v^a_{\mathrm{FM}} = 3390$ and 4988 m/s, hence in general $v^a_{\mathrm{AFM}} > v^a_{\mathrm{FM}}$.

In Fig. 4 we report the projection on Fe and Rh atoms of the vibrational density of states (VDOS) for the two analyzed magnetic phases. The Fe-projected VDOS can be compared with the experimental inelastic x-ray scattering (NRIXS) results of Ref. [23].

The overall softening of phonon modes and the reduction of the vibrational phase space occurring during the AFM → FM phase transition are likely to have a sizable effect on κ_L. These two effects, however, are in competition: while lower group velocities would tend to produce a smaller κ_L for the FM phase, narrower phonon phase space leading to depleted anharmonic scattering would tend to produce a larger κ_L for the same phase. To quantify the κ_L change associated with the FeRh metamagnetic transition and determine which of the two described effects is dominant (i.e., either volumetric expansion or phonon-phonon scattering enhancement), we performed DFT-based BTE calculations.

The thermal conductivity of FM and AFM FeRh expressed as a function of temperature is shown in Fig. 5(a). As it can be appreciated therein, the FM phase is more conductive than the AFM phase over the whole interval of investigated temperatures. Near the experimental metamagnetic transition temperature, $T_M = 350$ K, κ_L increases from 4.1 W m^{-1} K^{-1} in the AFM phase to 5.7 W m^{-1} K^{-1} in the FM phase, rendering a relative κ_L increase of ≈40%. At such temperatures—and, as a matter fact, for most materials at $T \gtrsim 20$ K—the dominant phonon-phonon scattering mechanism is umklapp-like, thus κ_L should decrease under

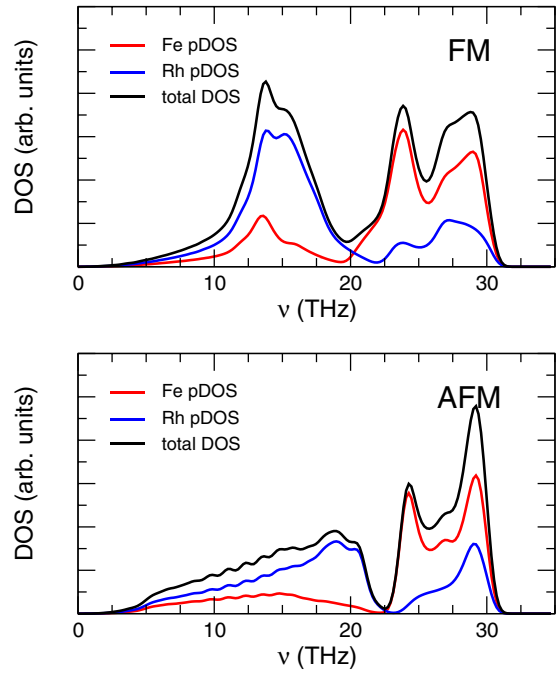

FIG. 4. Projection of the VDOS on Fe and Rh atoms and total VDOS for the FM and AFM cubic phases. Equivalent units and similar Gaussian broadening to that used in Ref. [23] have been employed here to facilitate comparisons.

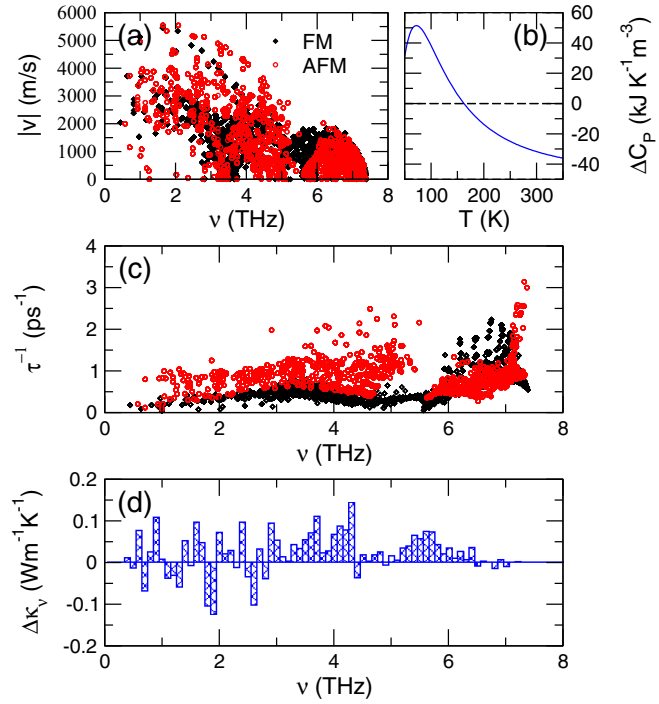

FIG. 6. (a) Module of the phonon velocities of FM and AFM FeRh expressed as a function of frequency. (b) Difference between the harmonic heat capacities estimated for FM and AFM FeRh, $\Delta C_P = C_P^{\mathrm{FM}} - C_P^{\mathrm{AFM}}$, expressed as a function of temperature. (c) Scattering rate expressed as a function of phonon frequency and computed as the inverse of the RTA phonon relaxation times [51]. (d) Frequency-resolved difference between the thermal conductivities of the FM and the AFM phases, $\Delta\kappa_{L,\nu} = \kappa_{L,\nu}^{\mathrm{FM}} - \kappa_{L,\nu}^{\mathrm{AFM}}$.

increasing T. However, for FeRh we predict an anomalous thermal conductivity increase close to T_M due to the AFM → FM phase transition [see the inset of Fig. 5(a)]. The κ_L cumulative estimated near T_M as a function of the phonon mean free path (mfp) is shown in Fig. 5(b). It is observed that, while in the AFM phase κ_L is determined by phonons with a mfp of at most 20 nm, in the FM phase κ_L saturates at l's as long as ∼80 nm, which is consistent with the larger thermal conductivity estimated for the FM phase.

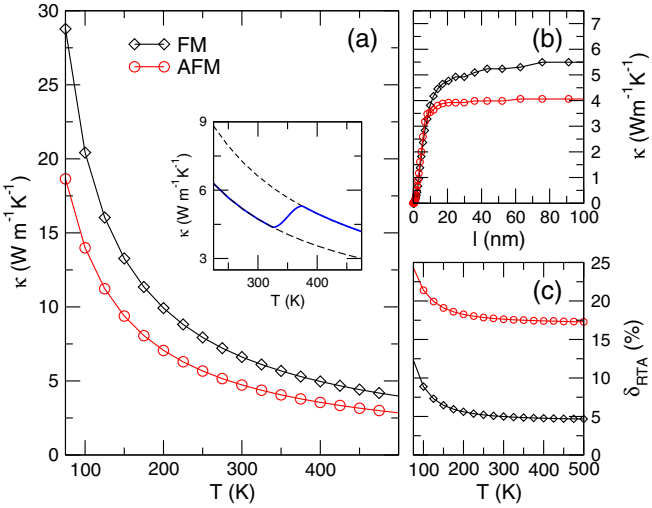

FIG. 5. (a) Estimated thermal conductivity expressed as a function of temperature and magnetic ordering. Inset: sketch of the κ_L change near T_M (the temperature range in which the transition occurs has been selected for visualization purposes only, thus in practice it may be narrower). (b) Cumulative thermal conductivity estimated at $T = 350$ K as a function of the phonon mean free path. (c) Relative deviation of the full iterative BTE solution from the RTA BTE solution, $\delta_{\mathrm{RTA}} = (\kappa_L^{\mathrm{iter}} - \kappa_L^{\mathrm{RTA}})/\kappa_L^{\mathrm{RTA}}$.

These results have been obtained from the iterative solution of the BTE. The reason for going beyond the RTA is that it erroneously considers momentum-conserving normal (N) processes to be resistive. Deviations from the RTA solution, therefore, can be interpreted as a measure of the importance of N-processes, which are core to non-Fourier-transport phenomena such as viscous heat flow and second sound [44–46]. This comparison is shown in Fig. 5(c). Interestingly, we found that N-processes depend strongly on magnetic ordering and are most critical for the AFM phase (i.e., deviations from the RTA solution are considerably larger for the AFM phase).

Our previous considerations on the FeRh phonon dispersions and κ_L's are fully ascertained by the results presented in Fig. 6. As was already anticipated, the phonon velocities of the AFM phase in general are larger than those of the FM phase [Fig. 6(a)]. A couple of exceptions appear in the low phonon frequency regions $\nu \lesssim 2$ THz (i.e., for some phonon modes $v_{\mathrm{AFM}} < v_{\mathrm{FM}}$) and $5.2 \lesssim \nu \lesssim 5.5$ THz (where $v_{\mathrm{AFM}} = 0 \neq v_{\mathrm{FM}}$). Also, in the low phonon frequency region $\nu \lesssim 2$ THz, the normalized density of phonon states is slightly larger for the AFM phase than for the FM phase, hence at

low temperatures ($T \lesssim 150$ K) the harmonic volumetric heat capacity, C_P, of the FM phase is larger [Fig. 6(b)]. Conversely, within the phonon frequency region $2 \lesssim \nu \lesssim 7.4$ THz, the normalized density of phonon states of the FM phase tends to be larger and hence its C_P becomes smaller at moderate and high temperatures. The estimated v and C_P values indicate that, at the harmonic level, the κ_L of the AFM phase should be larger than that of the FM phase [Eq. (1)], which contradicts the all-inclusive κ_L results shown in Fig. 5(a).

On the other hand, the phonon scattering rates enclosed in Fig. 6(c) clearly show that the phase space of phonon-phonon processes is larger for the AFM phase at most frequencies (with the exception of the narrow interval $5.2 \lesssim \nu \lesssim 5.5$ THz), a trait that goes in the direction of decreasing its κ_L as compared to that of the FM phase. Thus, among volumetric and phonon-phonon scattering effects, the latter are found to be the main responsible for the κ_L increase of ≈40% estimated from the AFM → FM phase transition [Fig. 5(a)]. The frequency-resolved thermal conductivity results shown in Fig. 6(d) are reassuring: the FM phase is most conductive for most frequencies with some exceptions appearing at the low-ν region of the spectrum.

Based on all these results, it can be concluded that the large κ_L change found for the metamagnetic transition of FeRh is driven by anharmonic spin-phonon couplings (i.e., large differences in the phonon-phonon scattering phase space between the AFM and FM phases). The main effect of switching to a different spin ordering is not simply to modify the phonon frequencies, but rather to increase the anharmonic phonon scattering by increasing the number of allowed collision processes. As a matter of fact, the conventional harmonic spin-phonon coupling leads to a softening of the phonon modes of the FM phase, thus reducing the overall κ_L increase from the AFM → FM transition. This is an important observation because it suggests that even larger magnetophononic effects than reported here could be observed in magnetic crystal where harmonic and anharmonic spin-phonon κ_L effects were not in competition (e.g., common T-induced FM—or AFM—to paramagnetic phase transitions [37]).

Finally, we mention that FeRh is a metallic alloy [47–49] and thus in practice electronic contributions to the total heat conductivity, κ_e, should be not negligible. In fact, by employing the Wiedemann-Franz law $\kappa_e = L_0 T \sigma$, where $L_0 = (\pi k_B)^2/3e^2$ and σ is the electrical conductivity, and the experimental σ data reported for AFM and FM FeRh in Ref. [20], we estimate an electrical heat conductivity of 6.1 W m^{-1} K^{-1} for the AFM phase and of 10.7 W m^{-1} K^{-1} for the FM phase at temperatures close to T_M. Since the electrical conductivity of FM FeRh is larger than that of AFM FeRh [20], the change in κ_e upon the AFM → FM phase transition is also positive and equal to ≈75%. Thus, for the total heat conductivity, $\kappa = \kappa_L + \kappa_e$, we predict a change of ≈60% for the FeRh metamagnetic phase transformation, and about 25% of such a variation stems from lattice contributions. Experimentally, therefore, in FeRh the magnetophononic effects reported in this work should not be counteracted by the also present electronic contributions to κ. At the same time, we note that in experiments where electronic thermal conduction could be considerably suppressed via nanostructuring (e.g., in metal-semiconductor interfaces like FeRh/$BaTiO_3$ [50]), the importance of the magnetophononic effects described here would be dominant.

V. MAGNETIC SYMMETRY BREAKING EFFECTS IN THE ESTIMATION OF THE THERMAL CONDUCTIVITY OF FeRh IN THE AFM PHASE

The calculation of the harmonic and anharmonic interatomic force constants (IFCs) within a real-space supercell approach is based on the finite-difference evaluation of force derivatives. To this end, once a conveniently large supercell is created, selected atoms are displaced. The total number of required displacements is of the order of $6N$, where N is the number of atoms in the unit cell. However, this large number of intensive DFT calculations can be reduced by taking advantage of the symmetry of the crystal lattice. This is what both PHONOPY [40] and THIRDORDER.PY [41], the codes that we use for the harmonic and anharmonic IFCs calculations, do. For instance, only one displacement is necessary to compute the phonon dispersion of FM FeRh, which has two atoms in the primitive cell.

This approach, however, faces a certain problem when dealing with AFM phases since the detection of symmetry performed by the mentioned codes is exclusively based on the position of the ions, and thus the further symmetry reduction caused by the presence of spin-up and spin-down ions generally is not accounted for. To bypass this problem, for the detection of symmetry and calculation of the inequivalent displacements, we have introduced a fictitious chemical species to force PHONOPY and THIRDORDER.PY to distinguish spin-up Fe atoms from spin-down Fe atoms. Such a numerical *trick* is not required for systems in which AFM spin ordering already introduces significant structural changes as compared to the FM spin ordered phase; however, in the particular case of bulk FeRh, only the volume changes appreciably in moving from the AFM to the FM phase, hence it is not possible to distinguish them by relying exclusively on their atomic positions.

To assess the importance of this technical detail and procedure, we have recalculated the thermal conductivity of the cubic AFM phase without employing the stratagem described above. In doing this, all Fe atoms look equivalent, like in the FM phase, and fewer calculations are needed due to the artificial higher symmetry of the system (i.e., two displacements instead of three for harmonic IFC calculations, and 304 instead of 464 for anharmonic IFC calculations). Our results, displayed in Fig. 7, show that by wrongly assuming a higher symmetry for the AFM phase, its thermal conductivity turns out to be largely overestimated. As a matter of fact, the flawed AFM κ_L turns out to be even larger than the κ_L estimated for the FM phase, which is at odds with the full discussion presented in Sec. IV. This finding is not surprising, though: by ignoring the symmetry reduction brought about by AFM spin ordering, the increase in phase space leading to the proliferation of phonon-phonon collisions is totally neglected. Therefore, to a first approximation, within such an incorrect scheme the AFM phase is merely a disguised FM phase (i.e., all Fe atoms are equivalent) with a smaller volume (hence the larger and wrongly estimated κ_L value).

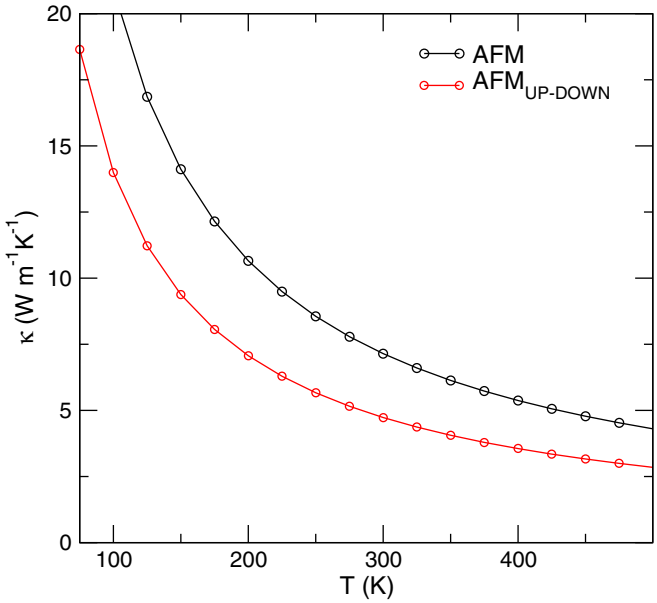

FIG. 7. Thermal conductivity of the AFM phase expressed as a function of temperature. The calculations have been performed by explicitly distinguishing spin-up from spin-down Fe atoms (red symbols) and by considering that all Fe atoms are equivalent (black symbols).

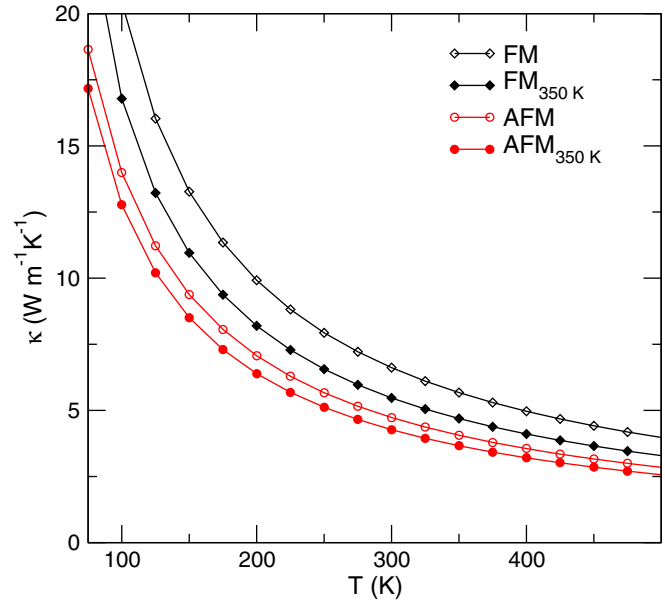

FIG. 8. Thermal conductivity of bulk FM and AFM FeRh expressed as a function of temperature. The thermal volumetric expansion estimated at 350 K is somehow taken into consideration in the κ_L calculations (filled symbols). Analogous results obtained for constrained zero-temperature volumes are shown for comparison (empty symbols).

VI. EFFECT OF VOLUMETRIC EXPANSION ON THE ESTIMATION OF FeRh THERMAL CONDUCTIVITIES

The standard procedure for *ab initio* calculation of thermal conductivities, which is the one followed in the present work, involves the computation of zero-temperature phonon dispersions and scattering rates; subsequently, the obtained phonon states are populated according to the Bose-Einstein statistics. Thus, the effects of temperature are only explicitly accounted for in the filling up of vibrational excitation levels.

In Sec. III, we explained how for a given crystal the T-induced variation of volume at fixed P can be estimated with the DFT-QHA method. For bulk FeRh, we have found that the volumetric thermal expansion of the FM phase is slightly larger than that of the AFM phase, thus at the experimental transition temperature the equilibrium volume difference between the two phases is also somewhat larger (i.e., 1.78% at 350 K versus 1.64% at zero temperature). As discussed in Sec. IV, larger volumes tend to yield lower thermal conductivities, hence the κ_L of the FM phase may experience a certain reduction with respect to that of the AFM phase when volumetric thermal expansion effects are somehow taken into consideration.

To approximately quantify the possible impact of thermal expansion effects in the computation of κ_L, we calculated the harmonic IFCs of each FeRh phase at the equilibrium volumes estimated at the phase-transition temperature $T_M = 350$ K. Then, by using the previously obtained zero-temperature scattering rates, we recalculated the two thermal conductivities. In fact, our results presented in Fig. 8 evidence that the decrease in heat conductivity estimated for the FM phase at $V(T_M)$, as compared to the reference $V(0)$ case, is larger than that estimated for the AFM phase. For instance, at T_M the quantity $\delta\kappa_{\rm FM} \equiv \kappa^{\rm FM}_{350K} - \kappa^{\rm FM}$ amounts to -0.98 W m^{-1} K^{-1}, whereas $\delta\kappa_{\rm AFM}$ amounts to -0.40 W m^{-1} K^{-1}. As a consequence of such distinct behaviors, the κ_L increase predicted for the metamagnetic FeRh phase transition, although still sizable, turns out to be slightly smaller than that reported in Sec. IV, namely, $\Delta\kappa_L \sim 30\%$ (to be compared with $\sim$40%).

It is worth noting that the T-renormalized $\Delta\kappa_L$ value reported in this section, however, should be considered just as orientative since many uncontrolled approximations (e.g., what is the impact of the neglected volume expansion on the phonon scattering rates?) are involved in the calculations. A fully rigorous $\Delta\kappa_L$ calculation accounting for all possible sorts of temperature effects (e.g., T-renormalized lattice parameters and T-renormalized phonon frequencies and scattering rates) appears to be prohibitively difficult and time-consuming for us at the moment, thus we leave it for future work.

VII. CONCLUSIONS

In summary, based on first-principles DFT calculations, we report the likely existence of magnetophononic effects in bulk FeRh, a prototypical multicaloric material. We predict a significant increase in the lattice thermal conductivity of FeRh ($\approx$40%) upon the near room-temperature AFM $\rightarrow$ FM metamagnetic phase transition that also can be driven by external magnetic fields. The disclosed magnetophononic effects and anomalous FeRh κ_L behavior originate from a large variation of the phase space of phonon-phonon processes that are dominant over conventional harmonic spin-phonon

couplings, which alone would induce a κ_L reduction. Since the main physical mechanism underlying the magnetophononic effects disclosed here is the modulation of the phase space for phonon-phonon collisions triggered by magnetic ordering changes, we expect that similar magnetophononic effects will exist also in other families of materials in which akin AFM $\leftrightarrow$ FM phase transitions are known to occur [26–31]. The present study, therefore, opens up new avenues for the dynamical control of heat transport in functional materials, thus besides of its fundamental interest it may also provide useful guides for the design of emerging phonon devices.

ACKNOWLEDGMENTS

We acknowledge financial support by MCIN/AEI/10.13039/501100011033 under Grant No. PID2020-119777GB-I00, the "Ramón y Cajal" fellowship RYC2018-024947-I, and the Severo Ochoa Centres of Excellence Program (CEX2019-000917-S), and by the Generalitat de Catalunya under Grant No. 2017 SGR 1506. Calculations were performed at the Centro de Supercomputación de Galicia (CESGA) within action FI-2021-1-0007 of the Red Española de Supercomputación (RES). We thank Michael Wolloch and Jesús Carrete for useful discussions.

[1] N. Li, J. Ren, L. Wang, G. Zhang, P. Hänggi, and B. Li, Rev. Mod. Phys. **84**, 1045 (2012).
[2] J. F. Ihlefeld, B. M. Foley, D. A. Scrymgeour, J. R. Michael, B. B. McKenzie, D. L. Medlin, M. Wallace, S. Trolier-McKinstry, and P. E. Hopkins, Nano Lett. **15**, 1791 (2015).
[3] J. A. Seijas-Bellido, C. Escorihuela-Salayero, M. Royo, M. P. Ljungberg, J. C. Wojdeł, J. Íñiguez, and R. Rurali, Phys. Rev. B **96**, 140101(R) (2017).
[4] M. Royo, C. Escorihuela-Salayero, J. Íñiguez, and R. Rurali, Phys. Rev. Mater. **1**, 051402(R) (2017).
[5] E. Langenberg, D. Saha, M. E. Holtz, J.-J. Wang, D. Bugallo, E. Ferreiro-Vila, H. Paik, I. Hanke, S. Ganschow, D. A. Muller *et al.*, Nano Lett. **19**, 7901 (2019).
[6] D. Dangić, E. D. Murray, S. Fahy, and I. Savić, Phys. Rev. B **101**, 184110 (2020).
[7] J. A. Seijas-Bellido, H. Aramberri, J. Íñiguez, and R. Rurali, Phys. Rev. B **97**, 184306 (2018).
[8] J. A. Seijas-Bellido, I. J. Íñiguez, and R. Rurali, Appl. Phys. Lett. **115**, 192903 (2019).
[9] P. Torres, J. A. Seijas-Bellido, C. Escorihuela-Sayalero, J. Íñiguez, and R. Rurali, Phys. Rev. Mater. **3**, 044404 (2019).
[10] P. Torres, J. Íñiguez, and R. Rurali, Phys. Rev. Lett. **123**, 185901 (2019).
[11] C. Liu, P. Lu, Z. Gu, J. Yang, and Y. Chen, J. Phys. Chem. C **124**, 26144 (2020).
[12] G. Qin, Z. Qin, S.-Y. Yue, Q.-B. Yan, and M. Hu, Nanoscale **9**, 7227 (2017).
[13] P.-W. Ma, C. H. Woo, and S. L. Dudarev, Phys. Rev. B **78**, 024434 (2008).
[14] P.-W. Ma, S. L. Dudarev, and C. H. Woo, Phys. Rev. B **85**, 184301 (2012).
[15] X. Wu, Z. Liu, and T. Luo, J. Appl. Phys. **123**, 085109 (2018).
[16] L. Mañosa and A. Planes, Adv. Mater. **29**, 1603607 (2017).
[17] E. Stern-Taulats, A. Planes, P. Lloveras, M. Barrio, J.-L. Tamarit, S. Pramanick, S. Majumdar, C. Frontera, and L. Manosa, Phys. Rev. B **89**, 214105 (2014).
[18] E. Stern-Taulats, A. Gracia-Condal, A. Planes, P. Lloveras, M. Barrio, J.-L. Tamarit, S. Pramanick, S. Majumdar, and L. Manosa, Appl. Phys. Lett. **107**, 152409 (2015).
[19] C. Cazorla, Appl. Phys. Rev. **6**, 041316 (2019).
[20] M. A. de Vries, M. Loving, A. P. Mihai, L. H. Lewis, D. Heiman, and C. H. Marrows, New J. Phys. **15**, 013008 (2013).
[21] E. F. Bertaut, A. Delapalme, F. Forrat, G. Roult, F. De Bergevin, and R. Pauthenet, J. Appl. Phys. **33**, 1123 (1962).
[22] M. R. Ibarra and P. A. Algarabel, Phys. Rev. B **50**, 4196 (1994).
[23] M. Wolloch, M. E. Gruner, W. Keune, P. Mohn, J. Redinger, F. Hofer, D. Suess, R. Podloucky, J. Landers, S. Salamon *et al.*, Phys. Rev. B **94**, 174435 (2016).
[24] M. P. Belov, A. B. Syzdykova, and I. A. Abrikosov, Phys. Rev. B **101**, 134303 (2020).
[25] D. W. Cooke, F. Hellman, C. Baldasseroni, C. Bordel, S. Moyerman, and E. E. Fullerton, Phys. Rev. Lett. **109**, 255901 (2012).
[26] J. H. Lee and K. M. Rabe, Phys. Rev. Lett. **104**, 207204 (2010).
[27] S. Hidaka, H. Toyota, and N. Uchitomi, Appl. Phys. Lett. **110**, 132410 (2017).
[28] V. Taufour, U. S. Kaluarachchi, R. Khasanov, M. C. Nguyen, Z. Guguchia, P. K. Biswas, P. Bonfà, R. De Renzi, X. Lin, S. K. Kim *et al.*, Phys. Rev. Lett. **117**, 037207 (2016).
[29] J. R. Jeffries, R. L. Stillwell, S. T. Weir, Y. K. Vohra, and N. P. Butch, Phys. Rev. B **93**, 184406 (2016).
[30] Y. Y. Y. Nishihara and M. Tokumoto, J. Magn. Magn. Mater. **70**, 173 (1987).
[31] Q. Shen, I. Batashev, F. Zhang, H. Ojiyed, N. van Dijk, and E. Bruck, J. Alloys Compd. **866**, 158963 (2021).
[32] G. Kresse and J. Furthmüller, Phys. Rev. B **54**, 11169 (1996).
[33] P. E. Blöchl, Phys. Rev. B **50**, 17953 (1994).
[34] G. Kresse and D. Joubert, Phys. Rev. B **59**, 1758 (1999).
[35] Y. Zhang and W. Yang, Phys. Rev. Lett. **80**, 890 (1998).
[36] H. J. Monkhorst and J. D. Pack, Phys. Rev. B **13**, 5188 (1976).
[37] C. Cazorla, O. Diéguez, and J. Íñiguez, Sci. Adv. **3**, e1700288 (2017).
[38] J. Kim, R. Ramesh, and N. Kioussis, Phys. Rev. B **94**, 180407(R) (2016).
[39] L. H. Lewis, C. H. Marrows, and S. Langridge, J. Phys. D **49**, 323002 (2016).
[40] A. Togo and I. Tanaka, Scr. Mater. **108**, 1 (2015).
[41] W. Li, J. Carrete, N. A. Katcho, and N. Mingo, Comput. Phys. Commun. **185**, 1747 (2014).
[42] Y. Wang, Z. Lu, and X. Ruan, J. Appl. Phys. **119**, 225109 (2016).
[43] S. Maat, J.-U. Thiele, and E. E. Fullerton, Phys. Rev. B **72**, 214432 (2005).

[44] R. J. Hardy, Phys. Rev. B **2**, 1193 (1970).
[45] A. Cepellotti, G. Fugallo, L. Paulatto, M. Lazzeri, F. Mauri, and N. Marzari, Nat. Commun. **6**, 6400 (2015).
[46] M. Simoncelli, N. Marzari, and A. Cepellotti, Phys. Rev. X **10**, 011019 (2020).
[47] C. Koenig, J. Phys. F **12**, 1123 (1982).
[48] N. I. Kulikov, E. T. Kulatov, L. I. Vinokurova, and M. Pardavi-Horvath, J. Phys. F **12**, L91 (1982).
[49] Y. Hao, L. Zhang, and J. Zhu, Z. Naturforsch., A **75**, 789 (2020).
[50] Z. Q. Liu, L. Li, Z. Gai, J. D. Clarkson, S. L. Hsu, A. T. Wong, L. S. Fan, M.-W. Lin, C. M. Rouleau, T. Z. Ward *et al.*, Phys. Rev. Lett. **116**, 097203 (2016).
[51] Within the full solution of the BTE, relaxation times and scattering rates are ill-defined. It is possible to define a generalized scattering rate as the projection of the vector mean free paths on the group velocities. This quantity, however, cannot be interpreted as a physical scattering rate. It is just a descriptor of how the phonon population of that mode deviates from the predictions of the RTA, and it can even be negative.